Supplemental Material: Evidence for phonon skew scattering in the spin Hall effect of platinum

G. V. Karnad,[1] C. Gorini,[2,*] K. Lee,[1] T. Schulz,[1] R. Lo Conte,[1,3] A. W. J. Wells,[4] D.-S. Han,[1,5] K. Shahbazi,[4] J.-S. Kim,[5,†] T. A. Moore,[4] H. J. M. Swagten,[5] U. Eckern,[6] R. Raimondi,[7] and M. Kläui[1,3,‡]

[1]*Institut für Physik, Johannes Gutenberg-Universität, Staudinger Weg 7, 55128 Mainz, Germany*

[2]*Institut für Theoretische Physik, Universität Regensburg, 93040 Regensburg, Germany*

[3]*Graduate School of Excellence "Materials Science in Mainz"(MAINZ), Staudinger Weg 9, 55128 Mainz, Germany*

[4]*School of Physics and Astronomy, University of Leeds, Leeds LS2 9JT, United Kingdom*

[5]*Department of Applied Physics, Eindhoven University of Technology, 5600 MB Eindhoven, The Netherlands*

[6]*Institut für Physik, Universität Augsburg, 86135 Augsburg, Germany*

[7]*Dipartimento di Matematica e Fisica, Roma Tre University, Via della Vasca Navale 84, 00146 Rome, Italy*

(Dated: March 22, 2018)

MATERIAL DEPOSITION

The material stack: Ta(4.0)|Pt(4.0)|Co(1.3)|AlO_x(2.0) (all thicknesses in nm) is deposited onto a Si|SiO_2 substrate by DC magnetron sputtering with a base pressure of $\approx 7\times10^{-8}$ mbar. The capping layer of AlO_x is obtained by plasma oxidation of the Al deposited on Co. The plasma oxidation is carried out in an in-situ isolated chamber for 10 min with 0.1 mbar oxygen background pressure at 15 W.

Deposition conditions		
Material	Working pressure (Pa)	Sputter power (W)
Tantalum	1.4	20
Platinum	0.29	60
Cobalt	1	20
Aluminium	1	20

The stack is characterized using MOKE microscopy and is found to exhibit a perpendicular magnetic anisotropy.

DEVICE FABRICATION

The thin film deposited on the Si|SiO_2 substrate is used to pattern the Hall bar structures. To perform the transport measurements we use e-beam lithography and ion milling to pattern Hall-bar devices (1-2 μm in width and 50 μm in length). In the first lithography step and milling process we define the Hall bars with small contact pads. In the second lithography step we define the larger contact pads (which overlap the small contact pads) and etch until (monitored using a mass spectrometer) we are in contact with the Pt under layer. The larger contacts for the Hall bars consist of Cr(10 nm)|Au(120 nm) which are sputter deposited after the second lithography step to make the final contacts.

RESISTANCE MEASUREMENT

The sheet resistivity of the sample is measured in two geometries: Hall-bar and thin-film sample. The residual resistivity of the samples is measured at 3 K. At this temperature, it can be assumed that the contribution to the resistivity is purely a result of the impurities

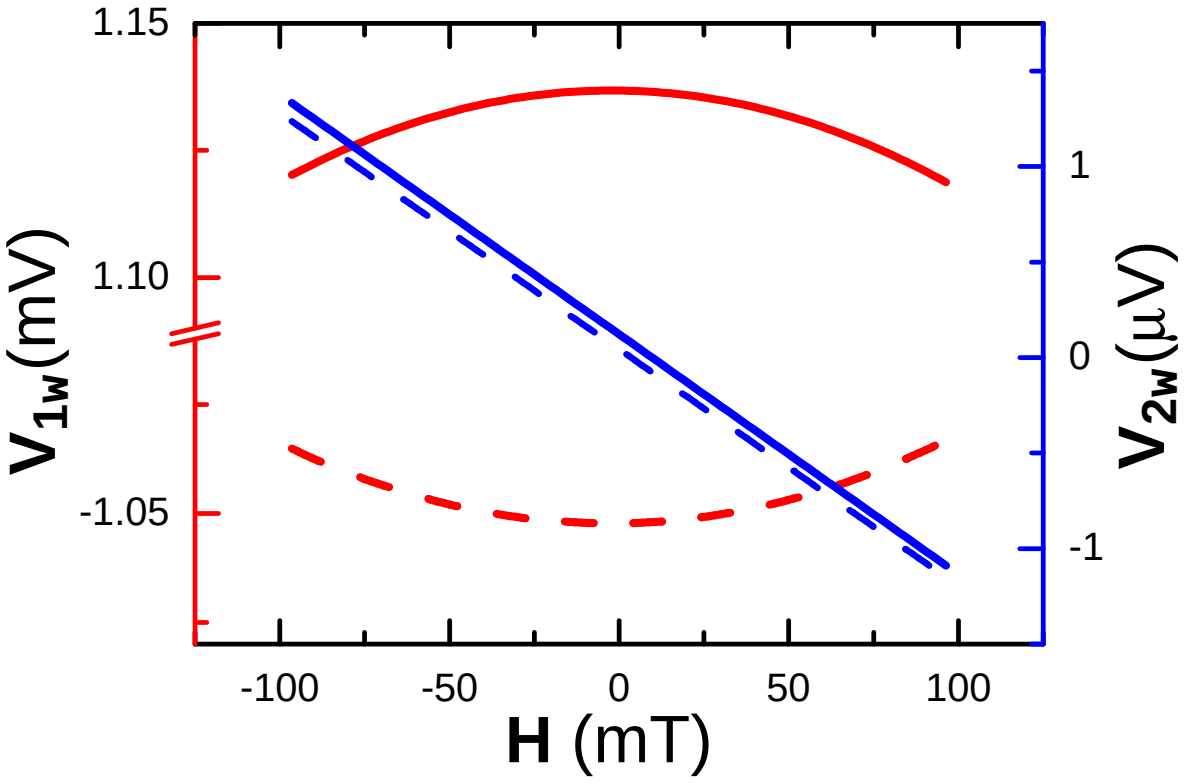

Fig. S1. Longitudinal scheme: First (red−−linear fit) and second harmonic (blue−−2nd order polynomial fit) voltages fitting for up (solid line) and down (dashed line) magnetization. Measured at 300 K

present in the system and which is not expected to change with temperature. Due to the fact that Pt has the smallest resistivity in the multilayer system, it can be expected that the majority of the current passes through this layer. The residual resistivity of the Hall-bar geometry is thus found to be 3.8 $\mu\Omega$cm. A van der Paauw [1] measurement is also performed on a thin film sample (2.5 mm x 2.5 mm), and we find the residual sheet resistivity to be 5.3 $\mu\Omega$cm.

SECOND-HARMONICS MEASUREMENT

The measurements are performed in a 3D vector cryostat. The 3D vector magnet set-up allows to address the magnetization in the complete 3-dimensional space. This allows us to unambiguously extract the appropriate current induced effective fields by studying the

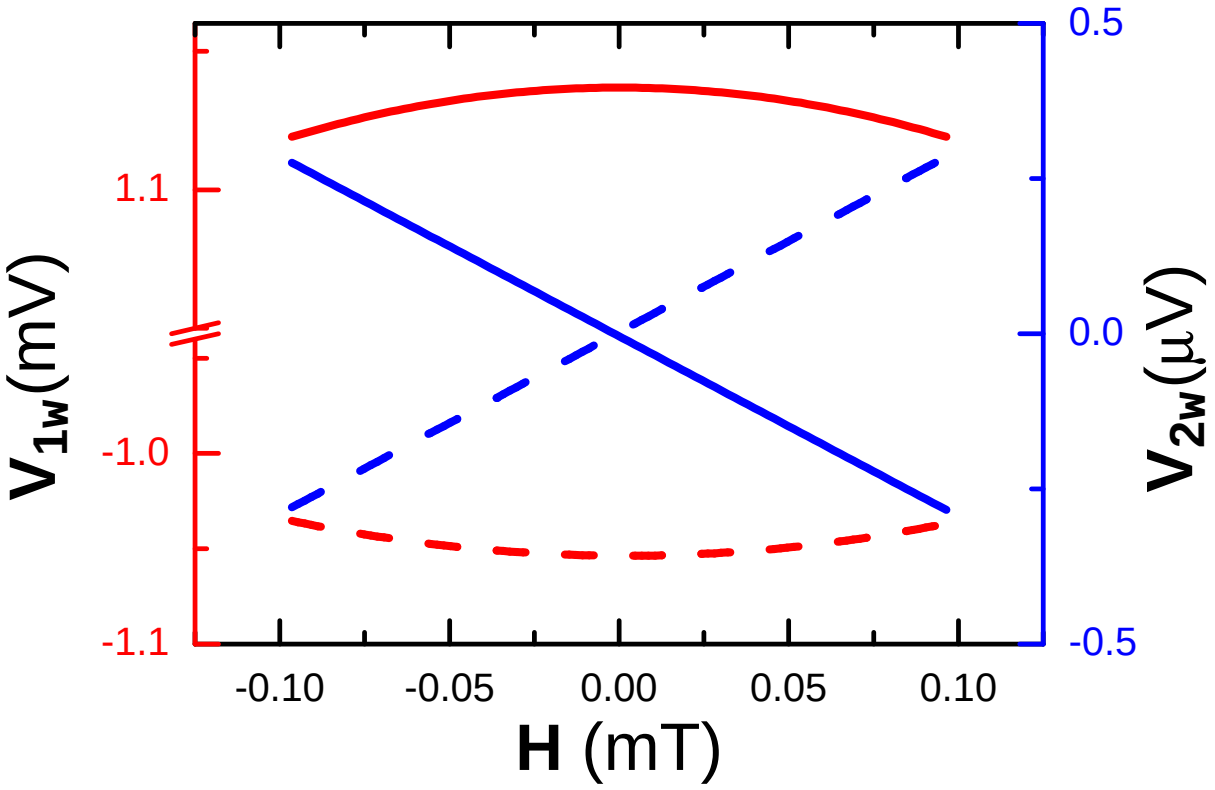

Fig. S2. Transversal scheme: First (red−−linear fit) and second harmonic (blue−−2nd order polynomial fit) voltages fitting for up (solid line) and down (dashed line) magnetization. Measured at 300 K.

angular dependence of the fields and the symmetry of the exerted torques. The injection of an ac current signal results in the perturbation of the magnetization in the ferromagnet away from its equilibrium position. This results in the change of the Hall voltage. To extract the SOT effective fields, the measurements are performed under the application of external magnetic fields in two schemes: 1. longitudinal: along the x-axis (damping-like), and 2. transversal: along the y-axis (field-like). In the longitudinal scheme, $V_{1\omega}$ exhibits a parabolic shape and its sign depends on the direction of the magnetization (Fig. S1). Results for the transversal scheme are identical. In case of the $V_{2\omega}$, in the transversal scheme it exhibits linear behavior, which has opposite slopes depending on the magnetization (Fig. S2). In the case of the longitudinal scheme they have the same slopes (Fig. S1) resulting from the symmetry of the torques. The effective fields can be extracted by measuring the first ($V_{1\omega}$) and second harmonic ($V_{2\omega}$) signal of the Hall voltage and is expressed by [2–4] Eqn.1, where

the term $B_{L,T}$ is the relation between $V_{2\omega}$ and $V_{1\omega}$ for both longitudinal and transversal directions:

$$B_{L,T} = \frac{\partial V_{2\omega}}{\partial H} \Big/ \frac{\partial^2 V_{2\omega}}{\partial H^2} \tag{1}$$

The variation of the Hall voltage has various contributions such as Nernst effect, Joule heating, anomalous Hall effect, and planar Hall effect. This is taken [3, 4] into account before extracting the spin-orbit torque effective fields. The final expression relating the hall voltage with the SOT effective fields (H_L and H_T) is given by [3, 4] Eqn. 2 and Eqn. 3, where $\xi = \frac{\Delta R_{PHE}}{\Delta R_{AHE}}$ is the ratio of the planar Hall effect resistance and the anomalous Hall effect resistance:

$$\Delta H_L = -2\frac{B_L \pm 2\xi B_T}{1 - 4\xi^2} \tag{2}$$

$$\Delta H_T = -2\frac{B_T \pm 2\xi B_L}{1 - 4\xi^2} \tag{3}$$

ADDITIONAL CONTROL MEASUREMENTS

a) Pt based sample

An additional control sample stack for "clean" Pt(Pt(4 nm)|Co(0.8 nm)|AlO_x(2 nm)) was grown to confirm the origin of the non-monotonic behavior observed in Fig. 3 (main manuscript). In comparison to the sample discussed in the manuscript, this was grown in a different sputter chamber (at University of Leeds) and the growth process was optimized accordingly. A thin film of Pt was used for the measurement of the resistivity, and we find a residual resistivity of 6.3 $\mu\Omega$cm (Fig. S7). We observe from Fig. S3 and Fig. S4 that the spin orbit torque measurements are consistent with the results obtained from the sample used for the main text and thus this system yields a reproducible and robust temperature dependence of the torques that is not very sensitive to the specific details of the growth (working pressure, sputter power etc.: which tends to vary slightly from deposition chamber to deposition chamber). This confirms that the observation is not unique to the growth process in one single chamber and is reproducible in a "clean" Pt based sample. Fig. S5 and Fig. S6 confirm the non-monotonous behavior of the spin Hall resistivity as a function

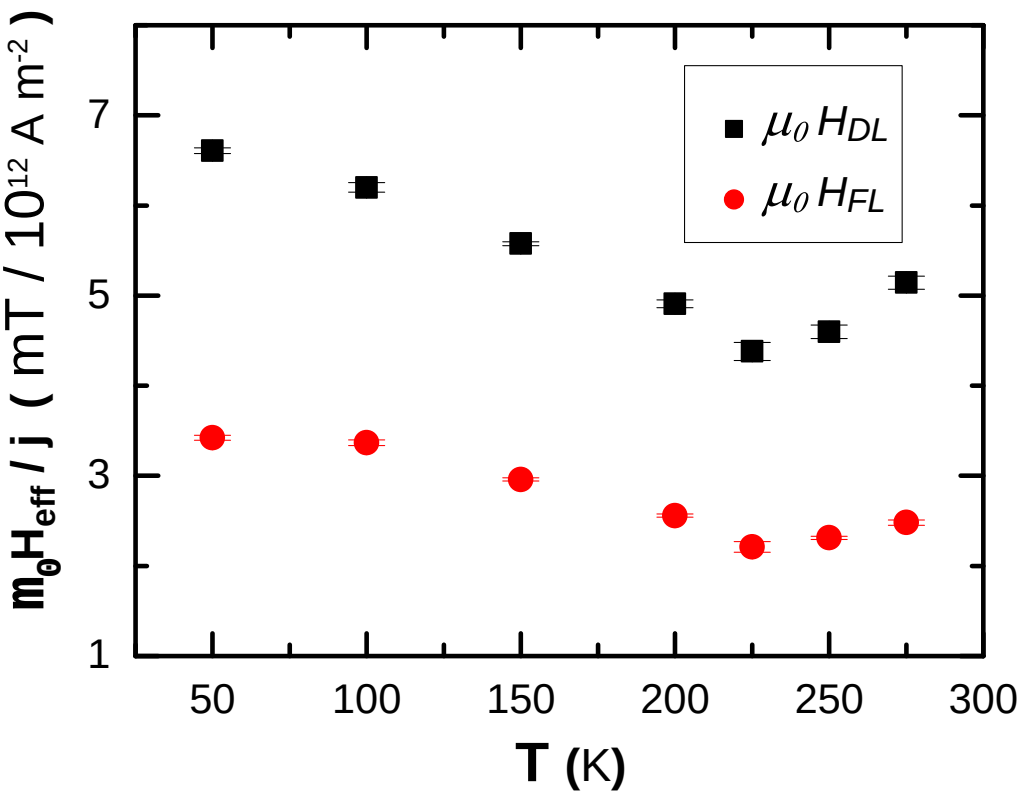

Fig. S3. The efficiency of the damping-like ($\mu_0 H_{DL}$) and field-like ($\mu_0 H_{FL}$) spin orbit torque effective field is given as a function of temperature. The behavior is found to be in agreement with that found for the other Pt based sample presented in the main manuscript (Fig. 3).

of total resistivity. This prevents the application of a simple linear equation (as done in Ref. [24] of the main manuscript) to describe the evolution of the SHA with temperature.

b) Ta based sample

The temperature dependence of the SHA, extracted from the spin-orbit torques, was measured also in a sample of tantalum (|Ta(5 nm)|CoFeB(1 nm)|MgO_x(2 nm)). The Ta sample is used to measure the evolution of the SHA as a function of temperature in a sample with higher residual resistivity (136.52 $\mu\Omega$cm). We observe that despite the linear increase of the resistivity (Fig. S7) in the 50−−300 K range, the SHA remains rather constant (Fig. S4). This is in line with the theoretical expectation that one is expected to

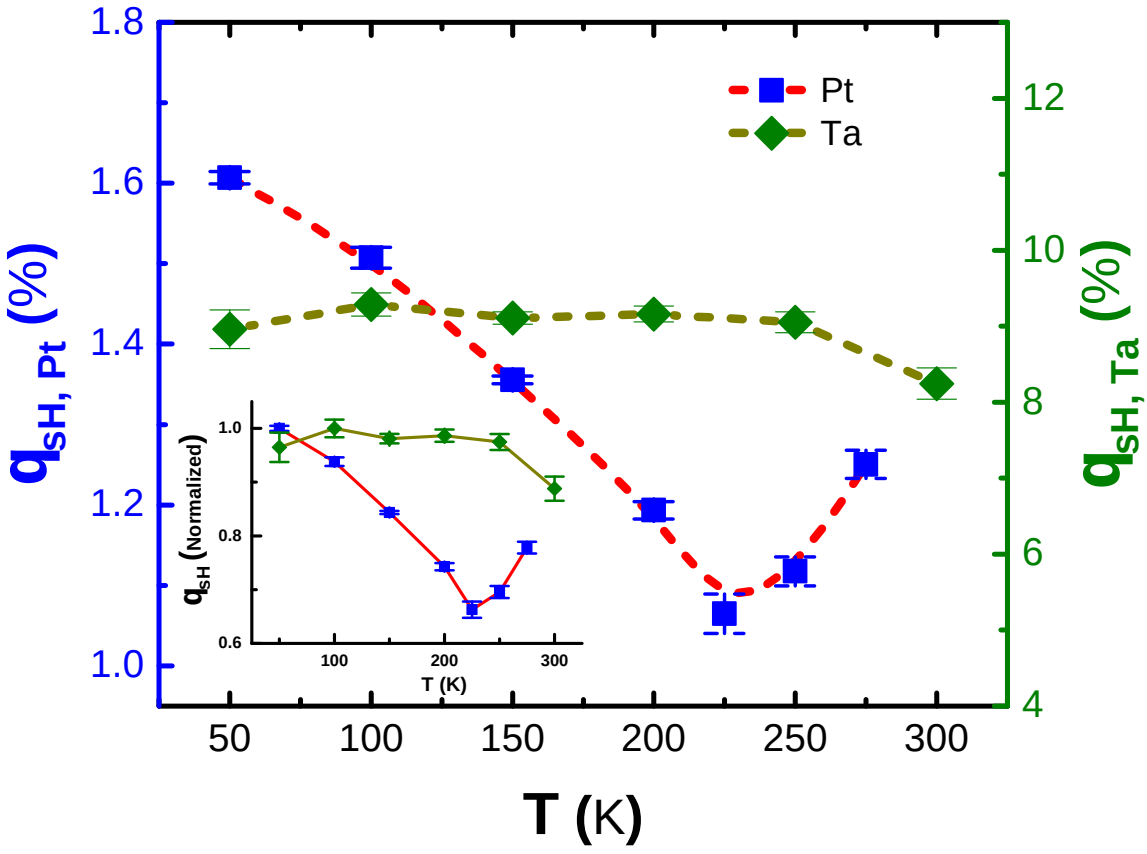

Fig. S4. Temperature dependence of the effective spin Hall angle ($\theta_{sH,Pt}$) in an additional sample of platinum (|Pt(4 nm)|Co(0.8 nm)|AlO_x(2 nm)) and tantalum (|Ta(5 nm)|CoFeB(1 nm)|MgO_x(2 nm)). We clearly see the non-monotonic behavior around T_D also found in the other Pt based sample presented in the main manuscript (Fig. 4).The inset shows the main figure with normalized θ_{sH}.

observe the contribution of phonon skew scattering in low resistivity samples.

TEMPERATURE SCALING OF THE SPIN HALL ANGLE

We discuss in more detail the derivation of the temperature behavior of the spin Hall angle (SHA), as sketched in Fig. 5 of the main manuscript. The discussion is based on the kinetic equations built in Refs. [5, 6], and on the phonon skew scattering theory from Ref. [7].

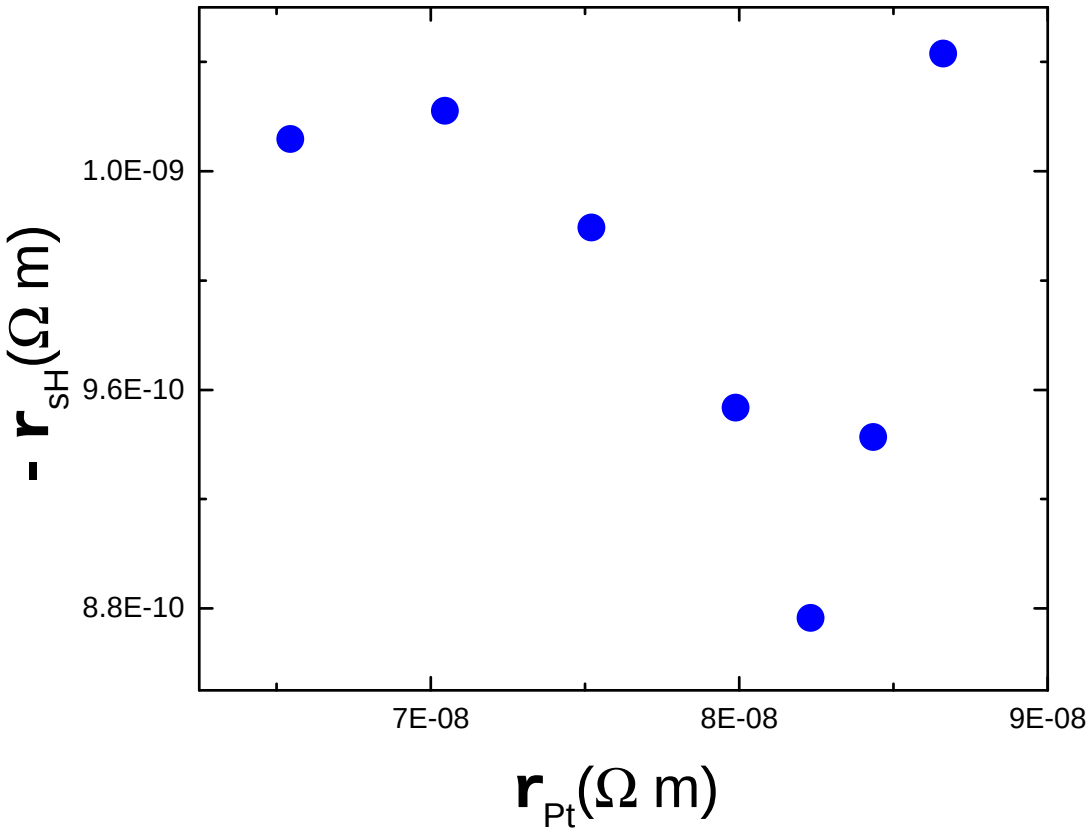

Fig. S5. Spin Hall resistivity versus total resistivity in Pt (6.3 $\mu\Omega$cm). The behavior (observed for both Pt films) clearly highlights the non-monotonic behavior of the SHA as well, and thus cannot be modeled with the simple linear equation.

Purely extrinsic spin Hall conductivity

Consider a sample where skew scattering, with impurities and with phonons, is the only source of the spin Hall effect. One solves the kinetic equation looking for the z-polarised spin current flowing along y, J_y^z, in response to an electric field E_x. This yields

$$J_y^z = \tau \left[\frac{\pi N_0 v_0}{\tau_i} - \frac{3\pi \Lambda g N_0 T}{\tau_{ph}} \right] \frac{(\lambda p_F)^2}{4} \sigma_D E_x \tag{4}$$

where $1/\tau = 1/\tau_i + 1/\tau_{ph}$ is the scattering rate due to electron-impurity ($1/\tau_i$) and electron-phonon ($1/\tau_{ph}$) scattering, λ an effective spin-orbit coupling constant, N_0 the density of states at the Fermi energy, v_0 the spatial average of the impurity potential ($\approx 1/2N_0$ for a Thomas-Fermi-screened impurity), g and Λ respectively the electron-phonon and phonon-

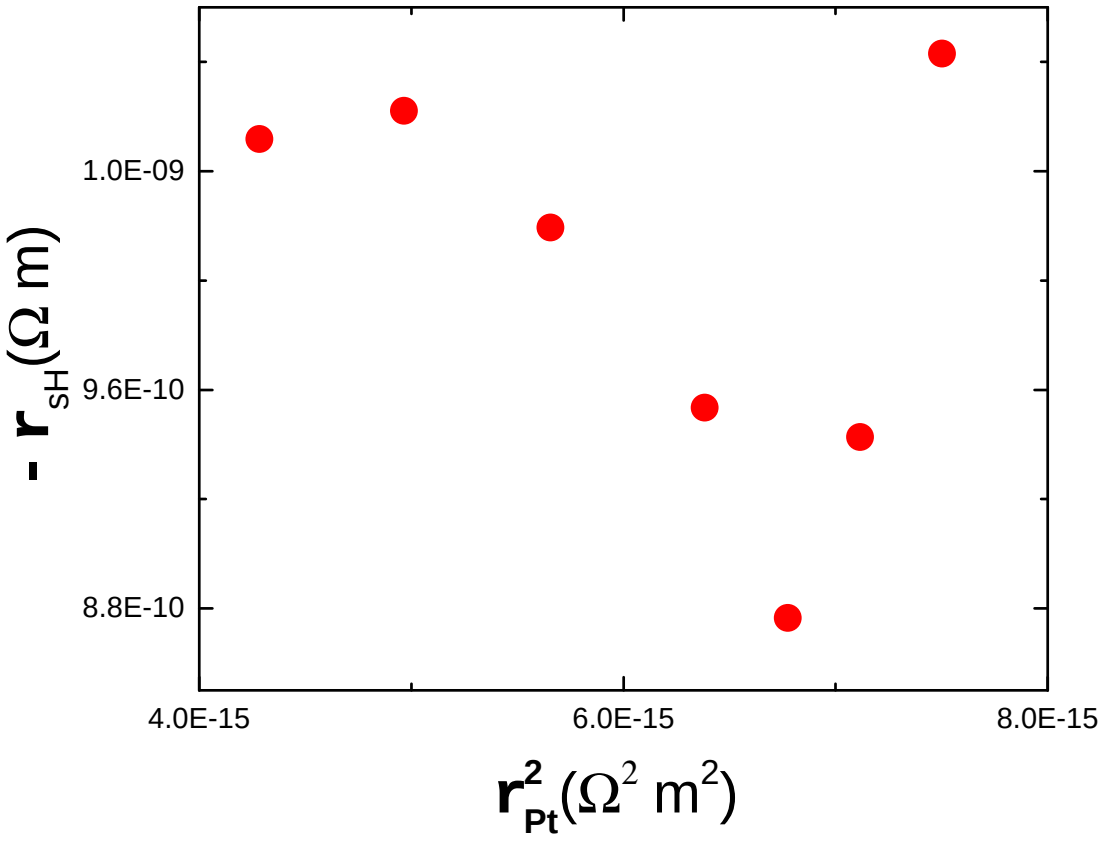

Fig. S6. Spin Hall resistivity versus the square of the total resistivity in Pt (6.3 $\mu\Omega$cm). The behavior (observed for both Pt films) again highlights the non-monotonic behavior of the SHA, and thus cannot be modeled with the quadratic equation either.

phonon coupling constants, and σ_D the Drude conductivity $eN_0v_F^2\tau$ (notice the lack of e^2, since we are dealing with spin, and not charge, currents). From the above one can write the skew scattering spin Hall conductivity as

$$\sigma_{sH}^{ss} = \frac{\pi N_0 v_0}{1+\tau_i/\tau_{ph}}\sigma_D \left[1 + \underbrace{\frac{3\gamma}{2\pi}\left(2\pi a/\lambda_F\right)^{3/2}}_{C_2\sim\mathcal{O}(1)} \tau_i/\tau_{ph}\,\frac{T}{\epsilon_F}\right]\frac{(\lambda p_F)^2}{4}. \tag{5}$$

The ratio $\tau_i/\tau_{ph} = [\rho(T) - \rho^{imp}]/\rho^{imp}$ is accessible by simply measuring $\rho(T)$ and looking at its residual $T = 0$ value ρ^{imp}. The numerical factor C_2 is positive and can be roughly estimated as being of order 1 (here a is the distance between ions, while γ is the Grüneisen

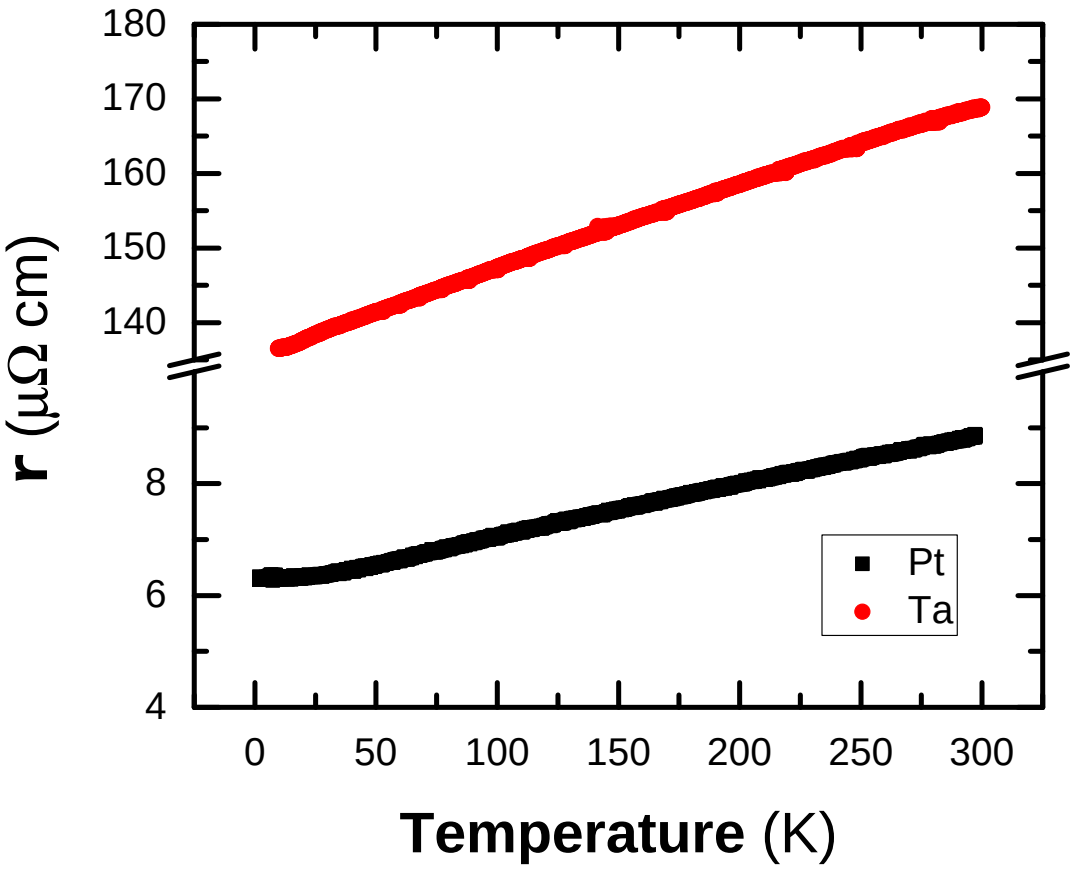

Fig. S7. Resistivity of Pt (6.3 $\mu\Omega$cm) and Ta (137 $\mu\Omega$cm) thin films measured as a function of temperature. They are found to behave linearly as expected in the 50−300 K temperature regime probed for the spin orbit torques.

parameter, typically ≈ 3). In the $T \to 0$ limit one obtains

$$\sigma_{sH}^{ss,0} = \underbrace{\pi N_0 v_0 \frac{(\lambda p_F)^2}{4}}_{C_1} \sigma^{imp} \tag{6}$$

showing the known result that skew scattering from impurities is proportional to the $T = 0$ conductivity $\sigma^{imp} = 1/\rho^{imp}$. It is possible to rewrite Eq. (5) as

$$\sigma_{sH}^{ss} = \frac{C_1}{\rho^2}\left[\rho^{imp} + C_2 \frac{T}{\epsilon_F}\left(\rho - \rho^{imp}\right)\right]. \tag{7}$$

When the temperature grows, the spin Hall conductivity decreases reaching a constant asymptotic value at $T \to \infty$. The flattening of the curve takes place at a temperature T_2

defined by

$$\rho^{imp} = C_2 \frac{T_2}{\epsilon_F} \Big[\rho(T_2) - \rho^{imp} \Big] \tag{8}$$

which implies that phonon skew scattering starts dominating over impurity skew scattering. T_2 is of the order of room temperature, but the precise value of C_2 depends on many material parameters and cannot be accurately estimated.

Adding an intrinsic contribution

One can introduce a temperature-independent intrinsic contribution σ_{sH}^{int}. Assuming as usual that extrinsic and intrinsic channels work in parallel, $\sigma_{sH} = \sigma_{sH}^{ss} + \sigma_{sH}^{int}$, this yields the full spin Hall conductivity

$$\sigma_{sH} = \sigma_{sH}^{int} + \frac{C_1}{\rho^2} \left[\rho^{imp} + C_2 \frac{T}{\epsilon_F} \left(\rho - \rho^{imp} \right) \right] \tag{9}$$

and resistivity

$$\rho_{sH} \approx -\sigma_{sH} \rho^2 = -\sigma_{sH}^{int} \rho^2 - C_1 \left[\rho^{imp} + C_2 \frac{T}{\epsilon_F} \left(\rho - \rho^{imp} \right) \right]. \tag{10}$$

Contact with Eq. (4) in the main manuscript is established identifying

$$\theta_{sH}^{ss,imp} = C_1, \quad \theta_{sH}^{ss,phon}(T) = C_1 \, C_2 \, \frac{T}{\epsilon_F} \quad \theta_{sH}^{int,0} = \sigma_{sH}^{int} \rho^{imp} \equiv C_3. \tag{11}$$

Scenario I: Clean sample

Consider a sample with very low residual resistivity, such that

$$C_1 > C_3 > 0, \tag{12}$$

having assumed positive C_1, C_3 to be definite (the same will be done in the following). The SHA starts by $C_1 + C_3$ at zero temperature, and has to reach a minimum at $T \approx T_1$, defined by

$$\frac{C_1 \, \rho^{imp}}{\rho(T_1)} = C_3 \rho(T_1). \tag{13}$$

Beyond T_1 an increase with (asymptotic) slope $\propto C_3$ sets in. This lasts roughly until the temperature T_2 is reached, see Eq. (8). From this point on phonon skew scattering dominates impurity skew scattering, and the SHA slope increases by a factor $\propto C_1 C_2$. In a standard

metal like Pt one expects $T_2 > T_D$, but nothing precise can be said unless an accurate value for C_2 is given – this requires precise knowledge of both electron-phonon and phonon-phonon interaction strength. On the other hand, $T_1 < T_D$ is likely, as T_1 is set by the ratio C_1/C_3, which are both $T = 0$ properties of the sample.

Scenario II: Dirty sample

When the residual resistivity is higher, so that

$$0 < C_1 < C_3, \tag{14}$$

the SHA has a much simpler, monotonic temperature behaviour: it increases with (asymptotic) slope $\propto C_3$ up to T_2, where the steepness increases by a factor $\propto C_1 C_2$. Once more, without accurate knowledge of the various material parameters the precise behavior cannot be given. Indeed, in a certain parameter range the decrease of the extrinsic term and the increase of the intrinsic one could compensate each other over a certain temperature range, yielding a constant SHA therein.

Remarks on low temperatures

While phonon skew scattering has to vanish for $T \to 0$, the exact form of the approach to zero is not yet known. This is an open and interesting subject for future research, which however does not change the qualitative discussion above.

* cosimo.gorini@physik.uni-regensburg.de

† now at: DGIST Research Center for Emerging Materials, DIGST, Daegu, 42988, Republic of Korea

‡ klaeui@uni-mainz.de

[1] L. van der Pauw, Philips Res. Rep. **13**, 1 (1958).

[2] U. H. Pi, K. W. Kim, J. Y. Bae, S. C. Lee, Y. J. Cho, K. S. Kim, and S. Seo, Appl. Phys. Lett. **97**, 162507 (2010).

[3] K. Garello, I. M. Miron, C. O. Avci, F. Freimuth, Y. Mokrousov, S. Blügel, S. Auffret, O. Boulle, G. Gaudin, and P. Gambardella, Nat. Nanotechnol. **8**, 587 (2013).

[4] M. Hayashi, J. Kim, M. Yamanouchi, and H. Ohno, Phys. Rev. B **89**, 144425 (2014).

[5] C. Gorini, P. Schwab, R. Raimondi, and A. L. Shelankov, Phys. Rev. B **82**, 195316 (2010).

[6] R. Raimondi, P. Schwab, C. Gorini, and G. Vignale, Ann. Phys. (Berlin) **524**, 153 (2012).

[7] C. Gorini, U. Eckern, and R. Raimondi, Phys. Rev. Lett. **115**, 076602 (2015).